

# First Measurements with a Scintillating Fiber Microdosimeter

Beatriz Fernandes<sup>1,a</sup>

<sup>1</sup>Faculdade de Ciências da Universidade de Lisboa, Portugal

Project supervisors: J. G. Saraiva, D. R. Guerreiro

October 18, 2022

**Abstract.** A scintillating fiber microdosimeter prototype is being designed and built by the LIP Dosimetry group. Microdosimetry aims at measuring the dose distribution at a cellular level in order to produce radiobiologic maps that relate radiation dose with biological effects. This paper describes the steps required in the preparation and installation of a fiber module, the main sensitive part of the microdosimeter. The main steps are: plastic scintillating optical fiber characterization, construction of a fiber module plane, assembly of the fiber module in the detector. In this paper is also suggested a possible quality control procedure and to conclude were made preliminary evaluations of an experimental X-ray radiation setup.

**KEYWORDS:** Microdosimetry, radiobiology, optical fibers, detector

## 1 Introduction

### 1.1 Introduction

Radiobiology studies the effect of ionizing radiation on living cells, specifically how different types of radiation affect different cells and different regions of a cell. The Dosimetry group of LIP is developing a high-resolution scintillating fiber microdosimeter, using juxtaposed plastic scintillating optical fibers and a multi-anode PMT. Figure 1 stands out the main elements of this dosimeter.

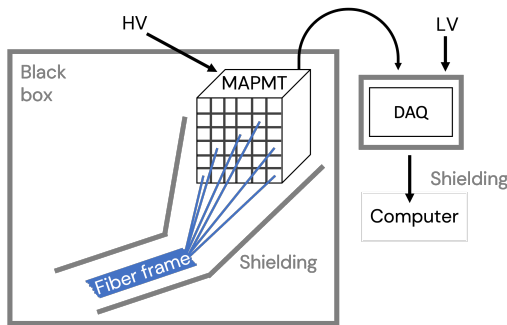


Figure 1: Scheme of the detector prototype.

### 1.2 Scintillating plastic optical fibers

The chosen fibers are the Kuraray SCSF-78. They are cylindrical, have a polystyrene (PS) core, a polymethylmethacrylate (PMMA) inner cladding and a fluorinated polymer (FP) outer cladding. The cladding has a lower refractive index compared to the core ( $n_{core} = 1.59$ ;  $n_{inner\ cladding} = 1.49$ ;  $n_{outer\ cladding} = 1.42$ ). A large fraction of the produced light is refracted but when the incidence angle is bigger than the critical angle ( $72.4^\circ$ ), the light is not refracted anymore but totally reflected, propagating along the fiber at the speed of light ( $c/n$ ), with  $c$  the speed of light in vacuum and  $n$  the medium index of refraction, as illustrated in Figure 2. The SCSF-78 re-

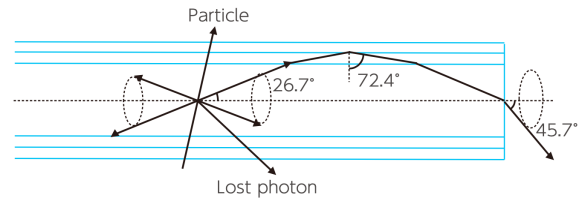


Figure 2: Total internal reflection diagram in a multi-cladding fiber [1].

spond to the deposition of energy by ionizing particles by producing scintillation light, peaking at the wavelength of 450 nm [1]. The option for plastic fibers is a result of their equivalence to biological tissue through their composition and density. Other characteristics like flexibility, radiation hardness and chemical inactivity make them an adequate material to use in the construction of radiation detectors for medical applications.

### 1.3 The microdosimeter

The main sensitive region of the detector are 64 juxtaposed scintillating plastic optical fibers with 1mm diameter held in place with a PVC frame; a 8x8 channels photodetector (H8500), powered by a high voltage source (HV: 800-1000 V); and the MARTA data acquisition system (DAQ) [2]. The parts are held together by a rigid structure made of POM (polyoxymethylene,  $(CH_2O)_n$ ) and PVC (polyvinyl chloride,  $(C_2H_3Cl)_n$ ) (detector skeleton). These materials are arranged so that the final detector volume is light tight, to eliminate any external sources that could interact with the fibres (background noise). Typically, fibers in this type of detector are covered with an opaque coating, but in this detector fibers have no coating, in order to not compromise tissue equivalence, cell adhesion to the fibers and compromise spatial resolution.

<sup>a</sup>e-mail: fc54921@alunos.fc.ul.pt

## 2 Main fiber characteristics

The optical characteristics of the fibers are measured before assembling them into the microdosimeter. These measurements are made with a fibrometer at LOMaC/LIP [3]. A LED based light source is used with the adequate wavelength. The controlled quantities are:

- Light yield
- Attenuation length
- Aluminium mirror reflectivity

The response uniformity of the fiber detector results from the combination of these three quantities. The test sample size is of 64 fibers collected from a larger set of fibers. It is important to note that although all output data is absolute, the result analysis must be done relatively to the reference fiber of the fibrometer, in order to minimize the impact of any external factors such as temperature, power network fluctuations, humidity, stabilization response, etc. The measurements are made with aluminized and non-aluminized fibers (a small set of fibers that had the aluminum mirror removed).

### 2.1 Light yield

The fibers' light yield is measured set distances for purpose of comparison to former and future measurements. Ideally, at the same distance, the response must be the same in all fibers; in reality, the measurement result is expected to show a normal distribution with a small spread (RMS<7%). This is to ensure the homogeneity of the output signal in response to a uniform radiation source.

### 2.2 Attenuation length

The probability of finding a particle at a distance  $x$  inside a material is calculated by Beer-Lambert law:

$$P(x) = e^{-x/L_{at}} \Rightarrow I_x = I_0 e^{-x/L_{at}} \quad (1)$$

where  $L_{at}$  is a parameter that is designated as an attenuation length and  $I_0$ . The formula tells us that after a travelled length equal to the attenuation length the intensity is dropped by  $1/e$ . Considering this, by measuring the output current of the fibers at various distances, it is possible to do an exponential fit whose attenuation parameter reveals  $L_{at}$ . The attenuation length is a limiting factor to consider when choosing fiber length, or even the fibers to be used, for the detector: it shouldn't be much longer than  $L_{at}$ , to reduce the signal attenuation before photodetection.

### 2.3 Aluminium mirror reflectivity

When radiation hits and deposits energy in the scintillating fibers, the scintillating photons can propagate in two directions: to the PMT, and away from the PMT. In order to capture the latter component, an aluminium mirror is placed at the further end of the fiber, for the light rays to be reflected. The process of coating the edge with aluminium is called aluminization. Fibers were aluminized

at LOMaC/LIP using a thin film technique known as magnetron sputtering [4] before the internship. The effect of the mirror can be added to the aforementioned equation (1), by adding a second term that comprises the additional length travelled by the scintillating photons and the reflectivity of the aluminum mirror:

$$I_x = I_0 e^{-x/L_{at}} + I_0 e^{-(L-x)/L_{at}} \times R \times e^{-L/L_{at}} \quad (2)$$

where  $L$  is the total fiber length and  $R$  is the mirror reflectivity. To verify this effect, response from aluminized and non-aluminized fibers are compared using once more the fibrometer. It is deemed important that these measurements are made with the same fibers, so that the only variable is the presence of the aluminum mirror. In order to carry out measurements with the non-aluminized fibers, the aluminum mirrors are removed with caustic soda from a small set of fibers (aqueous solution of sodium hydroxide, NaOH).

## 3 Fiber module prototype assembly

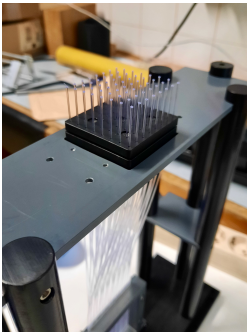
The fiber module assembly requires a set of meticulous steps in order to guarantee the correct adjustment of the scintillating optical fibres frame in its support skeleton. The skeleton, the internal structure of the microdosimeter, holds the fibers frame in place and positions the connector that guides the fibers to the MAPMT channels. The detector assembly steps are as follows:

1. Line up the fibers on the bottom frame (Figure 3 (a)), forming an array of aligned and juxtaposed fibers, using the assembly table.
2. Glue the top frame in order to prevent any fiber slippage.
3. Pass the fibers through the connectors' pinholes following a specific pattern decoupling cross-talk effects occurring at fibers level from the ones occurring at MAPMT level (Figure 4). Using the detector skeleton allows the correct fiber routing and length adjustment (Figure 3 (b)).
4. Trim the excess with a hot copper wire (Figure 3 (c)).
5. Glue the fibers to the connector's 1 mm pinholes (Figure 3 (d)).
6. Trim the excess to facilitate polishing (Figure 3 (e)).
7. Polish the surface using a diamond blade designed for the cut and polish of plastic fibers (Figure 3 (f)) at LOMaC/LIP.
8. Mount the MAPMT on the support skeleton (Figure 5).



(a)

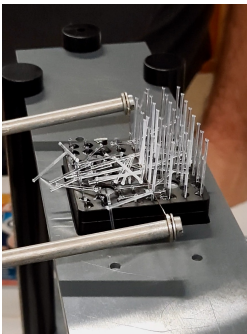
(b)



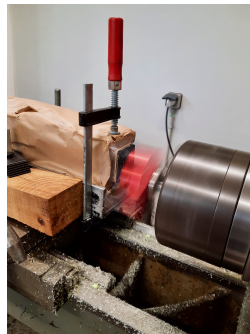
(c)



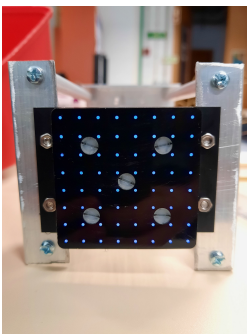
(d)



(e)



(f)



(g)



(h)

Figure 3: Fiber module assembly. (a) producing an aligned of juxtaposed fibers in the PVC frame; (b) routing each fiber into a specific pinhole in the MAPMT connector (Figure 4); (c) trimming the excess with a hot copper wire; (d) gluing the fibers to the connector's 1 mm pinholes; (e) trimming the excess before polishing; (f) polishing the surface; (g) view of the surface after polishing; (h) assembled fiber module.

1	9	17	25	33	41	49	57
5	13	21	29	37	45	53	61
2	10	18	26	34	42	50	58
6	14	22	30	38	46	54	62
3	11	19	27	35	43	51	59
7	15	23	31	39	47	55	63
4	12	20	28	36	44	52	60
8	16	24	32	40	48	56	64

Figure 4: Correspondence between fiber position in frame and MAPMT connector 8x8 matrix



Figure 5: Panorama of the assembled fiber module on the prototype skeleton.

## 4 Fiber module quality control and preliminary measurements

### 4.1 Fiber module quality control

After the assembly, a quality control procedure is implemented to evaluate the uniformity of the assembled module. Photographs of the fiber ends facing the MAPMT are taken illuminating the fiber plane with a dark light lamp, in an otherwise dark room. The setup (Figure 6) is assembled over an optics table, a lens is coupled to a computer camera and direct light from the lamp is avoided by using a black board. The horizontal plane (camera-detector) are naturally aligned due to the characteristics of the optics table where the setup was mounted. The vertical planes alignment should be improved in future measurements.

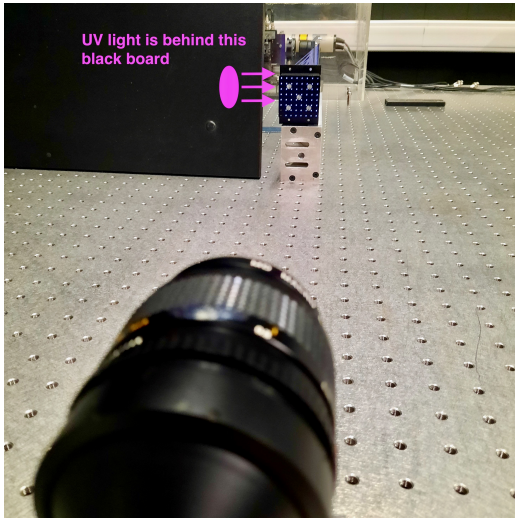


Figure 6: Photography setup to capture output light yield of all fibers while the frame is being irradiated by UV light.

In order to evaluate the effect of distance (homogeneity of the light field) in output variations, the UV lamp is placed 10, 25 and 45 cm away from the frame. Ten photographs are taken at each distance, along with five photos with the UV lamp switched off. The latter is subtracted to the former for background subtraction. Thus, it is possible to make a relative quantification of variations in light yield in all fibers.

#### 4.2 Preliminary measurements

Preliminary measurements are made with an X-ray tube (50 kV), a fiber covered with coating, a PMMA block, a lead brick and a PMT (Hamamatsu R647P). The setup is labeled in Figure 7. The PMT is then connected to an oscilloscope that is able to discriminate between signals by tens of nanoseconds (since the PMT R647P pulse time is of the order of 20 ns).

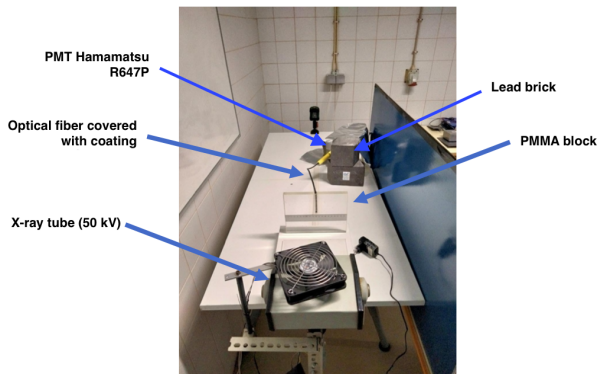


Figure 7: Preliminary setup to evaluate characteristic rate of an X-ray source available at FCUL.

## 5 Results and Conclusions

### 5.1 Fiber characterization

#### 5.1.1 Light yield

Light yield measurements at the same distance in all aluminized fibers appears to have a normal distribution as shown in Figure 8.

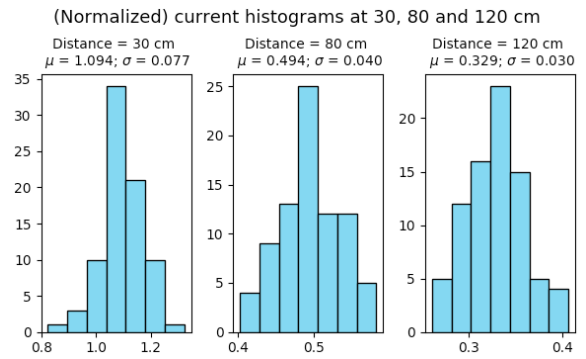


Figure 8: Current histograms at a given distance. The data is normalized to the reference fiber.

The standard deviation/mean ratio is around 8% at every distance, which is higher than expected. This may be due to the distance between the LED source and the fiber, as during these measurements it was greater than ideal.

#### 5.1.2 Attenuation length

Two functions are needed to better fit the original data, resulting in two attenuation lengths, one for each half of the total length. Figure 9 shows data from two fibers: one aluminized (gray) and one non-aluminized (black).

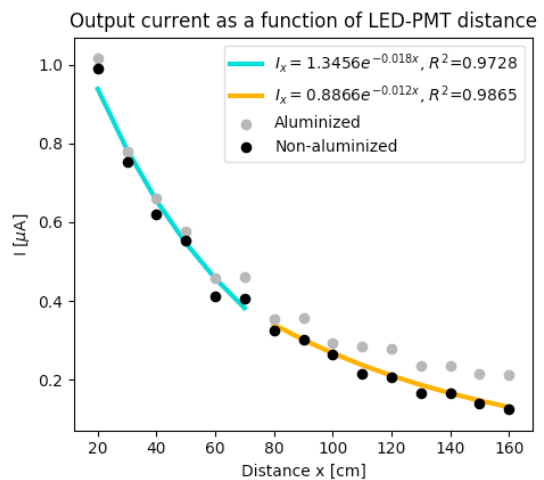


Figure 9: Measured output current from two fibers as a function of LED-PMT distance. Gray: aluminized fiber. Black: non-aluminized fiber. First and second fit functions of the non-aluminized fiber data are in blue and orange, respectively.

Both fits are calculated for 64 aluminized fibers, leading to an average "first"  $L_{at1} = 56.65$  cm ( $\sigma = 3.21$  cm) and a "second"  $L_{at2} = 119.50$  cm ( $\sigma = 7.56$  cm). The same is calculated for 3 non-aluminized fibers:  $L_{at1} = 54.16$  cm ( $\sigma = 0.77$  cm) and  $L_{at2} = 79.35$  cm ( $\sigma = 1.47$  cm). Note that  $\sigma$  in this report corresponds to standard deviation. Since the fibers used in the detector are about 30 cm long, attenuation is not a big problem in itself. The issue could lie with the geometry of the detector - some fibers need to be slightly curved to enter the connector, however, this results in a difference of no more than 1 cm in length.

### 5.1.3 Aluminium mirror

The effect of placing a mirror on the top end of an optical fiber increases its effective efficiency due to the increase in the number of photons collected or reduction in the number of photons otherwise lost by escaping through that open top end. The observed gain is in the order of 70% at  $x=160$  cm. The increase of effective light yield is also translated in an increase of the effective attenuation length as can be seen in Figure 9.

## 5.2 Fiber module quality control and preliminary measurements

### 5.2.1 Fiber module quality control

The collected images are processed using *ImageJ* [5] to compare light intensity between fibers. This measurement will combine the several characteristics of the assembled module: differences between fibers, glue effects, polishing effects and geometrical effects. For an 8-bit image, grayscale values vary between 0 (black) and 255 (white). So, the brighter the pixel, the higher its gray value. For every fiber in the picture, all gray values are added. Hence, the resulting sums can be compared. To simplify analysis, all values are normalized to the mean value, which in this case corresponds to 100. The resulting tables are shown in Figure 10. It is to be noted that the two fibers at the bottom left corner are broken, resulting in almost no signal.

Intensidades relativas em %

d = 10 cm								d = 25 cm								d = 45 cm							
72	72	75	74	81	80	75	78	97	93	101	98	112	109	111	110	100	94	104	94	113	109	110	108
76	84	81	95	89	78	78	84	93	100	98	110	115	95	106	103	94	102	102	112	113	96	103	105
88	94	86	94	64	94	99	98	100	107	99	102	74	102	115	111	98	103	97	107	76	99	115	119
98	107	103	114	108	120	108	110	100	106	107	115	116	123	121	119	96	106	106	118	118	124	119	116
107	108	113	116	117	107	109	118	100	100	112	107	114	99	109	110	103	94	108	106	114	97	107	110
108	120	113	110	120	130	124	129	96	106	99	95	110	112	113	115	97	102	100	94	109	112	111	118
5	113	113	130	127	117	127	129	5	89	90	104	101	88	105	103	5	90	91	109	100	88	108	107
9	119	103	124	121	128	124	106	3	91	81	96	95	98	99	89	5	89	77	95	92	100	99	90

Figure 10: Relative light intensity tables. Fibers brighter than average are represented with a green color and darker ones are red.

The tables in Figure 10 show that when the UV lamp is placed at a longer distance, because the field gets more uniform, the relative intensity pattern remains constant. At

10 cm, it is noticeable that the light field is stronger at the bottom and dimmer at the top. Differences in light yield between fibers can be algebraically compensated in the DAQ by using gain adjustments.

### 5.2.2 Preliminary measurements

The motivation of this preliminary measurement is to evaluate the time pulse pattern produced by the x-ray source. An snapshot of the output measured with an oscilloscope is shown in Figure 11. Most of the pulses appear separated at over 100 ns, however, some higher rates appear, which makes it difficult to measure different pulses. DAQ board limitations require at least a separation of 100 ns. The microdosimeter's PMT has better time response than the PMT used in the preliminary measurement setup, so a better performance is expected in that case. However it should be added that, in any case, the usage of attenuators (brass, lead, etc) is able to effectively reduce the rate and allow to proceed with the validation of the microdosimeter using this x-ray source.



Figure 11: Part of the PMT output in the oscilloscope. Pulses have a separation time greater than 100 ns, with the occasional appearance of higher rates.

## 6 Future improvements

The next steps for the development of the microdosimeter could be to use thinner fibers, to improve the spatial resolution. Another possible future implementation could overlap fiber planes or use square fibers, in order to minimize dead space due to cladding thickness. An important upgrade would be to combine two sets of fibers, perpendicular to each other, to get a two-dimensional distribution map. In terms of the measurements, in order to get a lower coefficient of variation when measuring light yield in the fibrometer, the distance between the LED source and the fiber should be shorter. For quality control, the alignment of the setup's vertical planes must be improved.

## Acknowledgements

I would like to express my sincere gratitude to João G. Saraiva and Duarte R. Guerreiro for their support and encouragement, and also to LIP, for providing students with

this incredible opportunity. The quality control of the assembled module was done with the help of colleagues at IA/FCUL: Alexandre Cabral, Manuel Abreu and Inês Leite. The characterization of the X-ray counted with the help of Luis Peralta (LIP/FCUL) and Pedro Assis (LIP/IST).

## References

- [1] L. KURARAY Co., *Plastic scintillating fibers online catalogue*, <http://kuraraypsf.jp/> (2022)
- [2] P. Assis, A. Blanco, P. Brogueira, M. Ferreira, R. Luz, *The marta (muon array with rpcs for tagging air showers) front-end acquisition system* (2018)
- [3] J. Saraiva, A. Wemans, M. Maneira, A. Maio, J. Patriarca, *IEEE TNS*, VOL. 51, NO. 3, JUNE 2004 (2004)
- [4] *LIP-LOMaC*, <https://lip.pt/?section=infrastructures&page=infrastructures-lomac&projectid=83&lang=en>
- [5] W. Rasband, *Imagej*, <https://imagej.nih.gov/ij/>, 1997-2018 (1997-2018)